Influence of Temperature and Pressure on Shape and Shift of Impurity Optical Bands in Polymer Glasses

Indrek Renge[†]

Institute of Physics, University of Tartu, Riia Str. 142, EE51014 Tartu, Estonia

Received: November 20, 2005; In Final Form: December 30, 2005

The shape, broadening, and shift of optical absorption spectra of molecular impurity centers in polymer glasses are considered in terms of inhomogeneous energy distributions and coupling of electronic transitions to vibrations. Persistent spectral hole burning was applied for frequency-selective probing of zero-phonon lines. The shift and broadening of spectral holes were studied between 5 and 50 K and by applying a hydrostatic He gas pressure up to 200 bar. Broadband absorption spectra were recorded between 5 and 300 K in poly(methyl methacrylate) and polyethylene. In addition to "normal" thermal broadening, due to the first- and second-order electron phonon coupling, several narrowing components were predicted on the basis of frequency dependent hole behavior. Thermal expansion of the matrix and the relaxation of local strains, previously accumulated on cooling below the glass temperature can lead to shrinking of the inhomogeneous width. A Voigt treatment of absorption band shapes reveals that the Gaussian component can indeed suffer remarkable narrowing. Inhomogeneous band shapes and the frequency-dependent thermal and baric line shifts were rationalized with the aid of a pair of two-body Lennard-Jones potentials. The shift of potential well minima is a crucial factor influencing solvent shifts, inhomogeneous band shapes, pressure shift coefficients, and quadratic electron phonon coupling constants.

1. Introduction

Organic dye molecules can possess remarkable optical properties, including large absorption cross-section, high luminescence emission rate and quantum yield, strong zero-phonon transitions, intrinsic photochemistry in solid solutions, etc. The spectrum at low temperature is mainly shaped by a convolution of inhomogeneous distribution function (IDF) of transition energies with vibronic sidebands accompanying zero phonon lines (ZPLs). Spectroscopic determination of IDF is straightforward by means of hole burning or selective fluorescence methods, if all guest particles possess identical spectra, except for the solvent shift of ZPLs.[1−3] However, the spectroscopy of single molecules reveals that in disordered environments the optical responses of impurity centers can be highly individual.[4−6] Single chromophores offer unique opportunities for probing the structure and dynamics of glasses, surfaces, nanoparticles, proteins, and other special environments.[7,8] Although devoid of such an ultimate resolution and selectivity, the burning of persistent spectral holes can address ensembles of chromophores with selected transition frequencies, and thus provide important insight into the disordered systems.[9,10] Hole burning is particularly convenient for observing small pressure shifts, reversible or irreversible temperature effects, and phonon sidebands.

The factors affecting guest spectra may be classified as the solvent shift phenomena and the electron phonon coupling (EPC) processes. Inhomogeneous band shape and pressure effects reflect the static aspects of the host structure. In the first approximation, linear EPC is responsible for phonon sidebands, whereas quadratic EPC manifests itself in the shift and broadening of ZPLs at temperatures above zero Kelvin. The studies of solvent shifts, vibronic frequencies and intensities, and quadratic EPC belong to well established, yet relatively unrelated fields of condensed phase spectroscopy. Large amount of theoretical work has been dedicated to solvent shifts in liquids[11−14] and inhomogeneous band shapes in glasses or defect crystals.[15−18] Linear EPC theory has been elaborated for zero-phonon transitions, such as Shpolskii lines, and for broad, multiphonon bands, e.g., the F-centers in alkali halides.[19−22] Theories of quadratic EPC have undergone considerable progress[23−27] and reached a general consistent form in nonperturbative approaches developed by Osadko[28] and Skinner.[29]

The applications of broad-band spectra have mainly been restricted to the spectrophotometric and luminescence methods of chemical analysis[30] and the creation of solvent polarity scales in organic chemistry.[31,32] The separation of homogeneous and inhomogeneous components of the spectra has rarely been attempted in the broad temperature range. In molecular materials the ZPLs lose intensity and broaden above 30 to 50 K, becoming inseparable from the phonon sidebands. If the ZPLs cannot be discerned, the obtaining of quadratic EPC parameters becomes difficult. The vanishing and broadening of ZPLs at higher temperature complicates also the study of the shapes of IDF. Both the line broadening and IDF are hard to measure in the spectra dominated by Franck−Condon progressions, even at the lowest temperatures.

A synthesis of the hole burning method and the broadband spectroscopy will be attempted in this work. Cold, isolated impurity molecules seeded in supersonic expansions[35−38] served as a reference state for the characterization of environmental shifts. Amorphous polymers and vitrified solvents were chosen, because they can be doped more readily with a large variety of different color centers than the metallic, ionic, or covalent network glasses. In a favorable case, the solute may introduce only a small perturbation to van der Waals glass structure and properties.

[†] Telephone: +3727-304800. Fax: +3727-383033. E-mail: indrek.renge@ut.ee.

10.1021/jp056714j CCC: $33.50
Published on Web 02/18/2006

Stable resonant holes were created in the absorption spectra of several tetrapyrrolic pigments, polycyclic hydrocarbons, and polymethine dyes in polymer host matrices. The broadening and the shift of holes upon changing temperature and pressure in the He gas atmosphere surrounding the sample was investigated as a function of burning frequency. The hole burning in soft glasses is limited to temperatures below 50 K as a result of vanishing ZPLs, spectral diffusion, or hole filling. Remarkably, the frequency dependencies of thermal and baric hole shifts are such as to produce a narrowing of the whole spectrum with increasing temperature. The extrapolation of the hole parameters was carried out with the aim of separating the contributions of inhomogeneous broadening and electron phonon coupling. Absorption spectra were recorded between 5 and 300 K and subject to a Voigtian fitting procedure, yielding the Gauss and Lorentz components. A strong deviation of 0−0 band shapes at low temperature from Gaussians is emphasized. A narrowing of Gaussians with rising temperature will be discussed in terms of hole behavior.

Successful spectral probing would critically depend on the completeness of the interpretation of spectra, requiring robust models to connect the host structure with the solvent shifts and the EPC parameters. We have recently proposed a simple approach to frequency dependent hole properties in terms of Lennard-Jones potentials.[33,34] A single configurational coordinate is introduced for the characterization of packing density in the vicinity of a guest molecule. In glasses, the intermolecular distances fluctuate with respect to the equilibrium values of the crystalline phases. The nonequilibrium nature of glasses is incorporated into the model by considering vertical transitions between pairs of hypersurfaces at different coordinate values, without the possibility of structural relaxation. The fluctuations of intermolecular coordinates depend on the glass temperature, according to a Boltzmann distribution of energies. The solvent shift can be expressed as a difference between the potential energies of connected states. The spectral distributions are obtained by plotting the ground-state energies as a function of solvent shifts. The response of IDF to a uniform compression or dilatation of the matrix can be obtained by scaling the intermolecular coordinate. A frequency dependence of baric line shifts follows from a difference between the first derivatives of the potentials.[33,34] Thermal line shift and broadening, caused by changes in the phonon frequencies can be associated with the second derivatives of Lennard-Jones functions, via the force constants. An agreement between the spectral behavior and the model can only be obtained for certain ratios of the equilibrium distances and the well depths, thus providing the Lennard-Jones parameters of the excited state.

2. Experimental Section

The pigments (see Figure 1 for structural formulas) and low-density polyethylene (density 0.915 g cm^{-3}, melting temperature 115 °C) were purchased from Aldrich. As a high molecular weight poly(methyl methacrylate) (PMMA) commercial Plexiglas was used. Chlorin and a phthalonaphthalocyanine $NcPc_3$ were available from our earlier work.[39] The 0.1−0.5 mm thick polymer films were cast from the solution as described in ref 40, where the details of measurements and data treatment can also be found. In short, the samples were fixed in a continuous flow optical cryostat CF1204, and the temperature was maintained within 1° with the ITC-4 temperature controller (both Oxford). Absorption spectra were recorded on a Perkin-Elmer Lambda 9 spectrophotometer with 1 nm slit width. Absorption spectra are presented and analyzed as measured, without correction either for the instrumental slit width nor the refractive index of air. The wavelengths were calibrated with 0.25 M aqueous solution of holmium chloride. The accuracy and long-term repeatability were better than 0.1 nm. In the spectra measured at different temperatures the baseline subtraction was performed carefully, because the small drifts result in large uncertainty of Voigtian fitting parameters.

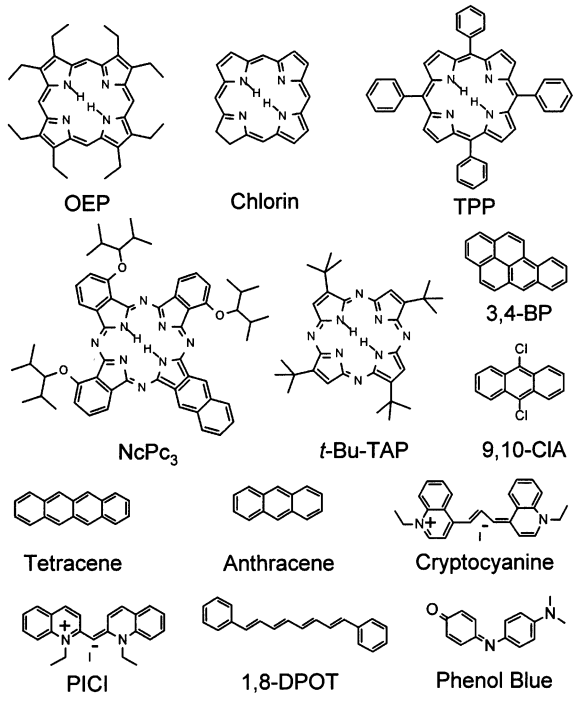

Figure 1. Chemical structures of probe molecules.

Spectral holes were burned with a LPD 3002E dye laser, pumped with 308 nm light from a LPX 100 excimer laser (both Lambda Physik). Holes were detected in transmission by scanning the dye laser with attenuated energy at 40 Hz pulse frequency, using a two-channel setup of a Molectron JD2000 Joulemeter/Ratiometer. The sensitive J3S-10 (10^9 V/J) probe was placed in the sample channel and the less sensitive one, J3-09 (10^3 V/J) served to measure the laser pulse energy. The hole widths were corrected for the laser line width by subtracting its double magnitude, 5 GHz, from the Lorentzian hole width. Pressure studies were carried out in a cylindrical cell of 20 mm in diameter, made of stainless steel and supplied with two sapphire windows. The sample volume of $2 \times 4 \times 4$ mm^3 was filled with gaseous He at 200 bar and cooled to 5 K, and the holes were burned. Subsequently the pressure was released step by step and the holes were recorded (for details see ref 41).

3. Results

3.1. Spectral Hole Burning. Tetrapyrrolic chromophores, occurring as heme pigments in the blood and tissue or as chlorophylls in photosynthetic membranes, are exceptionally well suited for hole burning in their metal-free state. Prototropic phototautomerism of the central pair of hydrogens, with quantum yields ranging from 10^{-4} (chlorin) to 10^{-2} (octaethylporphine), combined with the weak electron−phonon coupling (with Debye−Waller factors α from 0.5 to 0.90) facilitates the creation of deep and narrow spectral holes.[39] Hole burning is also possible in $^1L_b(\alpha)$ or $^1L_a(p)$ type transitions of polyarenes and in several symmetrical polymethine dyes (cryptocyanine) dis-

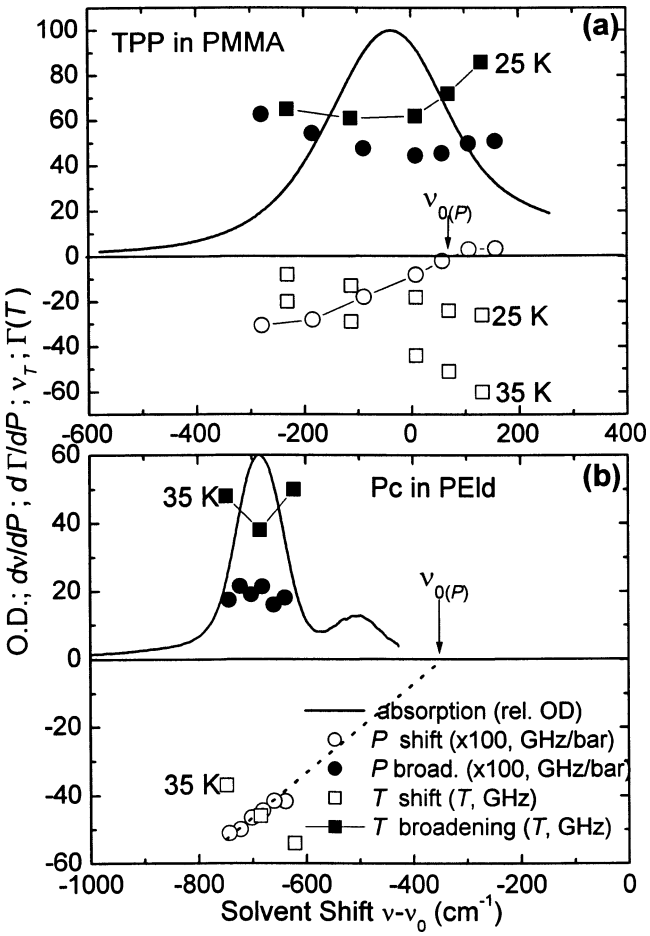

Figure 2. Absorption spectra of tetraphenylporphine in poly(methyl methacrylate) (a) and phthalocyanine in low-density polyethylene (b) at 6 K and frequency dependent properties of spectral holes: coefficients of pressure shift ($d\nu/dP$, ○) and broadening ($d\Gamma/dP$, ●), thermal shift (ν_T, □) and broadening ($\Delta\Gamma(T)$, ■) between 7 and 25 (35) K. In Pc the pressure shift (dotted line) extrapolates to zero at -345 ± 22 cm^{-1} below the 0−0 origin of free pigment ν_0 (15131.8 cm^{-1}, ref 38).

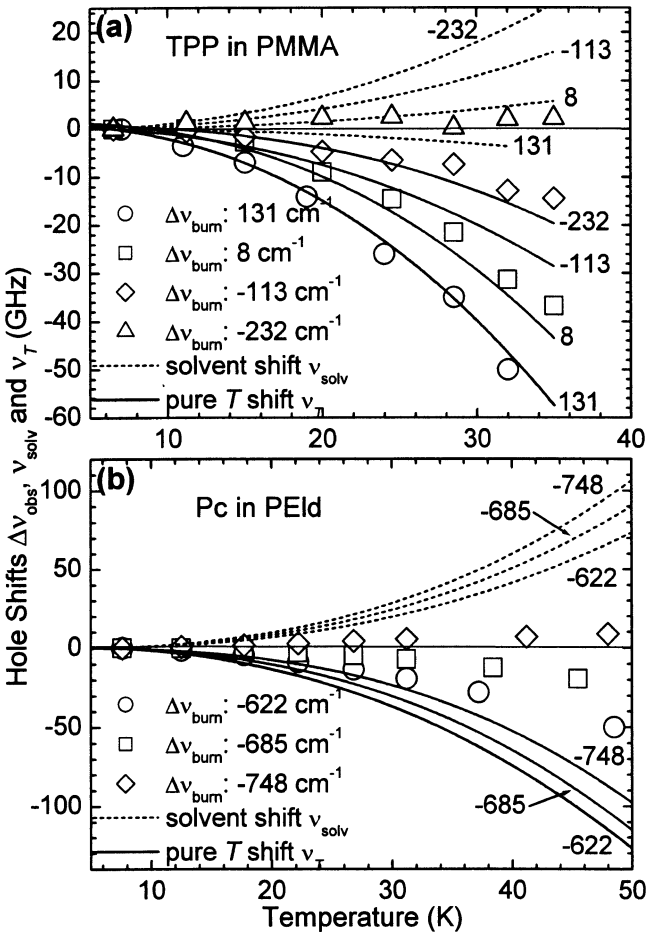

Figure 3. Thermal shifts of spectral holes burned in the absorption band of tetraphenylporphine in poly(methyl methacrylate) (a) and phthalocyanine in low-density polyethylene (b). Hole positions are indicated as absolute solvent shifts with respect to 0−0 frequencies in a vacuum in cm^{-1} units (15617 cm^{-1} for TPP and (ref 35) and 15131.8 cm^{-1} for Pc (ref 38)). Phonon induced shifts ν_T (thick lines) are calculated from the observed shift (open symbols) by subtracting the solvent shift due to the matrix expansion (dotted lines) (eq 19).

solved in a polar and hydrated matrix of poly(methyl methacrylate) (PMMA) that supports photobleaching.[41]

Temperature (T) and pressure (P) effects were investigated on deep holes burned over the inhomogeneous band at low T (from 5 to 7 K). Rather high burning doses were applied to improve the hole-to-background ratio, so that the initial width typically exceeds the quasihomogeneous width Γ_{qh} by a factor of 2−4. The shift and broadening are strictly proportional to the pressure change in the He gas atmosphere, and can, therefore, be characterized with coefficients $d\nu/dP$ and $d\Gamma/dP$, respectively. The shift coefficients $d\nu/dP$ show a well-known linear dependence on hole position, with a slope a and a frequency at which the pressure shift would disappear $\nu_{0(P)}$ (Figure 2):[41,42]

$$d\nu/dP = a(\nu - \nu_{0(P)}) \quad (1)$$

As a rule, $\nu_{0(P)}$ does not coincide with the resonance energy in a vacuum ν_0, and the pressure shift is not directly proportional to the solvent shift.[41,42]

Similar to pressure shifts, thermal hole shifts display a pronounced dependence on burning position (Figure 3), although with an opposite frequency dependence.[43] The observed T shift consists of a phonon-induced, pure thermal shift and a change of the solvent shift due to the expansion of matrix. It turns out that after subtraction of the latter from the observed shift, the resulting pure thermal shift ν_T has a similar, although a weaker, frequency dependence. Both thermal and baric shifts are to lower frequencies (negative, bathochromic) except for a few compounds (OEP, TPP). The extent of hole broadening, caused either by a change in pressure or temperature, has a relatively weak dependence on burning position (filled symbols in Figure 2).

Complex, nontrivial behavior of hole widths is shown for a phthalocyanine derivative $NcPc_3$ in low-density polyethylene (PEld) (Figure 4). Quasihomogeneous width Γ_{qh} is determined at a fixed T for shallow holes with relative depth of zero-phonon absorption less than 5%.[44] Following a warm-up to T_c and cooling to the initial (low) burning temperature, the width and, to some extent, the position of a hole, are not fully recovered. The residual broadening Γ_c reflects structural changes in a disordered system, referred to as a spectral diffusion.[40,45] Another peculiarity can be documented, when a hole that has been created at a higher T is monitored on gradual cooling. Instead of the expected shrinking (dotted line in Figure 4), a hole broadening is observed with lowering of the temperature. This Lorentzian broadening was assigned to nonuniform strains building up in the matrix as a result of a T change.[44] The thermal broadening of a single hole burned at a low T is the most complex one, containing information about the fast, reversible

TABLE 1: Absorption Band Maxima of Pigments in Poly(methyl methacrylate) at 6 K and Their Temperature Dependence[a]

pigment	ν_{max}, 6 K (cm^{-1})	ν_0 (cm^{-1})	$\Delta\nu_{max}$, 6 K (cm^{-1})	$\Delta\nu_{obs}$, 100/293 K (cm^{-1})	p (cm^{-1})	$d\nu_{max}/dP$ (GHz/bar)	ν_{solv}, 293 K (cm^{-1})	ν_T, 100/293 K (cm^{-1})	$a_2(\nu_T)$	$a_2(\Delta\nu_{obs})$
OEP	16238 ± 0.5	16056 ± 5	182	−10.2/−116	−128 ± 19	0.055	−5	−9.3/−111	2.28	2.25
chlorin	15814.3 ± 0.5	15912(j)	−98	−5.8/−74	−659 ± 20	−0.121	11	−7.7/−85	2.11	2.26
TPP	15579.3 ± 0.5	15617(j)	−38	−8.5/−98	−639 ± 40	−0.118	10	−10.4/−108	2.06	2.11
t-Bu-TAP	16239 ± 0.5	16326 ±9	−87	−10.5/−123	−988 ± 39	−0.26	23	−14.5/−146	1.89	2.09
$NcPc_3$[b]	13329.2 ± 0.5	13877 ±6	−548	−2.0/−21	−2087 ± 24	−0.451[c]	76	−14/−97	1.70	1.97
3,4-BP	24812 ± 1	25265(j)	−453	−4.0/−73	−1567 ±60	−0.235	20	−7.7/−93	2.29	2.51
9,10-ClA	24803 ± 1	25950(j)	−1147	2.0/−7	−4175[d]	−0.855	74	−11.4/−81	1.69	
tetracene	21071 ± 1	22403(j)	−1332	6/4	−5137 ± 207	(−1.0)	87	−9.8/−83	1.82	
anthracene[b,e]	38449 ± 2	41517 ± 40	−3068	8.4/160	−8077 ± 166	(−1.59)	267	−33/−107		
cryptocyanine	14017 ± 1	14630 ± 100	−613	0/−32	−3024 ± 286	(−0.58)	50	−9/−82	1.89	2.30
PICI	18905 ± 2	19716 ± 40	−811	−1/−15	−2964 ± 147	(−0.57)	49	−9/−64	2.07	4.64
1,8-DPOT[e]	24709 ± 3	27732 ± 40	−3023	34/183	−10024 ± 166	(−1.97)	171	4/12		1.63
Phenol Blue	16476 ± 2	19781 ± 134[f]	−3305	46/366	−6255 ± 556	(−1.22)	106	25/260	2.48	2.07

[a] ν_{max}, absorption band maximum at 6 K; ν_0, 0−0 transition energy in a vacuum, measured in a cold jet (j, refs 35−37, 41) or extrapolated from solvent shift data (refs 39, 42, 46); $\Delta\nu_{max}$, solvent shift $\nu_{max}-\nu_0$; $\Delta\nu_{obs}$, temperature shifts at 100 and 293 K; p, steepness of a plot of band maxima in liquid *n*-alkanes at at 293 K vs the Lorentz−Lorenz function (polarizability) of solvent (ref 41), $d\nu_{max}/dP$, pressure shift coefficient of a spectral hole burned at the band maximum (ref 41), the values in parentheses were estimated from eq 20; ν_{solv}, solvent shift component of the thermal shift $\Delta\nu_{obs}$ at 293 K (eq 19); ν_T, pure thermal, phonon induced shift of band maxima at 100 and 293 K; $a_2(\nu_T)$ and a_2 ($\Delta\nu_{obs}$), temperature coefficients of the approximations of ν_T and $\Delta\nu_{obs}$ to a power law. [b] In low-density polyethylene. [c] For phthalocyanine. [d] For anthracene. [e] $S_2\leftarrow S_0$ transition. [f] Vertical, vibronic charge-transfer transition.

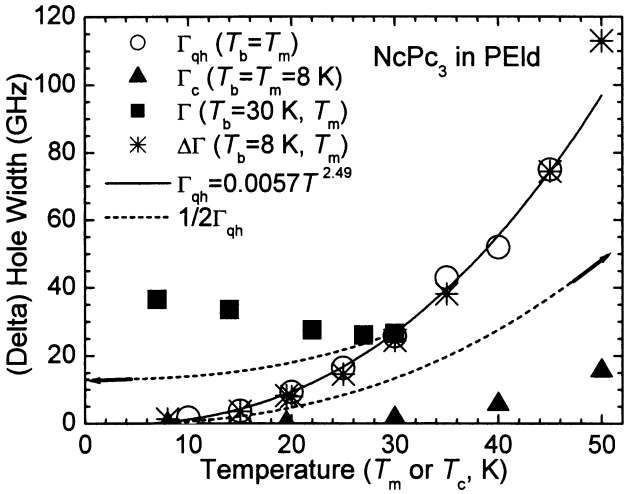

Figure 4. Different ways to measure hole widths, illustrated for asymmetric phthalocyanine $NcPc_3$ in a low-density polyethylene film, close to the absorption maximum (751 nm). Quasihomogeneous width Γ_{qh} (○) is obtained for holes burned and measured at the same temperature ($T_b = T_m$). Because of thermal, nanoscopic strains in the matrix, the broadening of a single hole on warming of the system ($T_b < T_m$) is (incidentally) close to Γ_{qh} rather than $^1/_2\Gamma_{qh}$ (∗). For the same reason, a spectacular broadening on cooling ($T_b > T_m$) appears (■). If the temperature is raised to T_c and lowered again down to burning temperature for the measurement ($T_b = T_m$), the broadening by spectral diffusion Γ_c is obtained (▲).

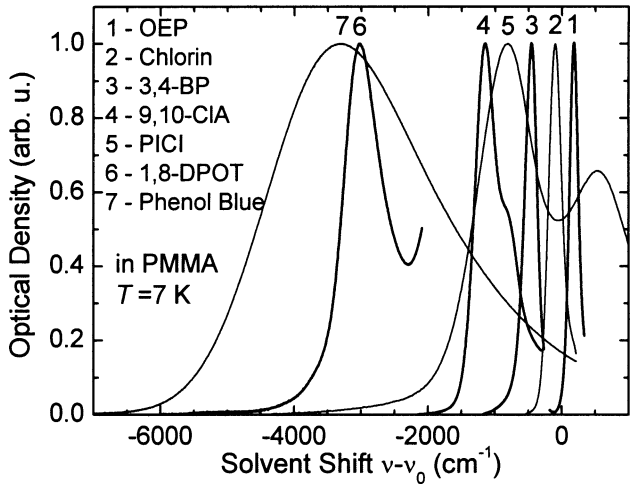

Figure 5. Normalized absorption spectra of porphyrins (1, 2), polycyclic hydrocarbons (3, 4), linear chromophores (5, 6), and a charge-transfer compound (7) in PMMA films at 7 K, presented in the scale of absolute solvent shifts vs the 0−0 frequency in a vacuum (see Table 1).

(homogeneous line width, Γ_h) and slow, irreversible dynamics (Γ_c), in addition to a strain-induced, reversible contribution.

3.2. Temperature Dependence of Absorption Spectra. Absorption spectra of several representatives of one- and two-dimensional π-electronic chromophores, such as polyenes, polymethine cations, polycyclic aromatic hydrocarbons, and tetrapyrroles are illustrated in Figure 5. Absolute solvent shifts of band maxima $\Delta\nu_{max}$ span from −3300 to +200 cm^{-1} (Table 1) and the widths vary between 145 and 2500 cm^{-1} (Table 2). With increasing negative $\Delta\nu_{max}$, the inhomogeneous width is expected to become larger. However, the correlation between the bandwidth and the solvent shift is generally weak (see Figure 6 in ref 42), because several factors mask this relationship. Fluctuating (bond) dipole−dipole interactions can produce a huge spread of solvent shifts of both signs, as compared to a relatively small electrochromic shift originating from a reaction field. Another important mechanism of inhomogeneous broadening arises as a result of intramolecular factors, such as the conformational flexibility of phenyl substituents in tetraphenylporphine or the twisting of terminal aromatic cycles in the open-chain polymethine dyes (cryptocyanine, PICI) (Figure 1). Additional broadening in PICI and 1,8-diphenyloctatetraene (1,8-DPOT) can be ascribed to the excitation of intramolecular soft modes, originating from the floppiness of molecular structure. Huge bandwidth of 2500 cm^{-1} of a charge-transfer transition in Phenol Blue (*N*,*N*′-dimethylindoaniline) derives from a Franck−Condon envelope of the higher harmonics of high-frequency bond stretching vibrations (1000−1500 cm^{-1}), smoothed out by medium-frequency molecular modes (150−1000 cm^{-1}) and quasilocal modes (10−100 cm^{-1}) (Figure 5). In the spectra dominated by vertical Franck−Condon transitions, the adiabatic transition energy, its solvent shift, and the inhomogeneous bandwidth are difficult to measure, because of the vanishing 0−0 line.

Thermal broadening and the shifts to opposite directions are illustrated for octaethylporphine (OEP) and 1,8-DPOT in PMMA (Figure 6). The band maxima ν_{max}, the 0−0 transition

TABLE 2: Absorption Bandwidths of Pigments in Poly(methyl methacrylate) at 6 K and Their Temperature Dependence[a]

pigment	2hwhm (Δ100/293 K), cm^{-1}	fwhm (Δ293 K), cm^{-1}	Γ_G (Δ293 K), cm^{-1}	Γ_L (Δ100/293 K), cm^{-1}	2hwhm/fwhm	Γ_G/Γ_L (293 K)	a_2(2hwhm)	$a_2(\Gamma_L)$
OEP	161 ± 1 (1.5/64)	163.3 (75)	136.3 (−29.5)	46.2 (14.2/121)	0.986	2.95 (0.64)	2.93	1.95
chlorin	229.4 ± 1 (1.5/36.8)	240.5 (38.8)	214 (−12)	29.3 (8.5/73)	0.954	7.30 (1.97)	2.94	1.74
TPP	277 ± 1 (17/119)	275 (115)	173 (−71)	180 (20/220)	1.01	0.96 (0.26)	1.67	1.96
t-Bu-TAP	329 ± 1 (10/103)	312 (102)	206 (−4)	210 (18.2/146)	1.05	0.98 (0.57)	2.14	1.95
$NcPc_3$[b]	145.2 ± 1 (4.5/32)	145.4 (27)	124 (−14)	43 (10/67)	0.999	2.88 (1.0)	2.32	2.05
3,4-BP	247 ± 2 (6/83)	226.5 (92)	158 (−158)	150 (13/193)	1.09	1.05 (0)	3.20	2.42
9,10-ClA	362 ± 2 (19/162)		324 (−38)	76 (15.3/290)		4.26 (0.78)	2.20	2.34
tetracene	315 ± 2 (13/95)	325 (127)	252 (−35)	110 (17/190)	1.03	2.29 (0.72)	2.56	2.22
anthracene[b,c]	489 ± 4 (40/307)		323 (298)	328 (−3/60)		0.98 (1.60)	2.27	
cryptocyanine	488 ± 2 (12/96)	586 (132)	468 (35)	23 (7.0/106)	0.83	20.3 (3.9)	2.46	2.35
PICI	1072 ± 4 (33/250)		835 (125)	420 (35/244)		1.99 (1.45)	1.75	1.81
1,8-DPOT[c]	575 ± 5 (35/248)		341 (227)	362 (5/75)		0.94 (1.3)	1.84	2.78
Phenol Blue	2512 ± 5 (50/426)	2976 (400)	2419 (360)	0	0.84	∞	2.20	

[a] 2hwhm, double value of the half-width at half-maximum on the red side of the band at 6 K, where the broadening at 100 and 293 K is indicated in parentheses; fwhm, full-width at half-maximum; Γ_G and Γ_L, the Gauss and Lorentz components of the Voigtian fitting of the low-frequency half of the spectrum; a_2, temperature coefficients of the approximations to power laws. [b] In low-density polyethylene. [c] $S_2 \leftarrow S_0$ transition.

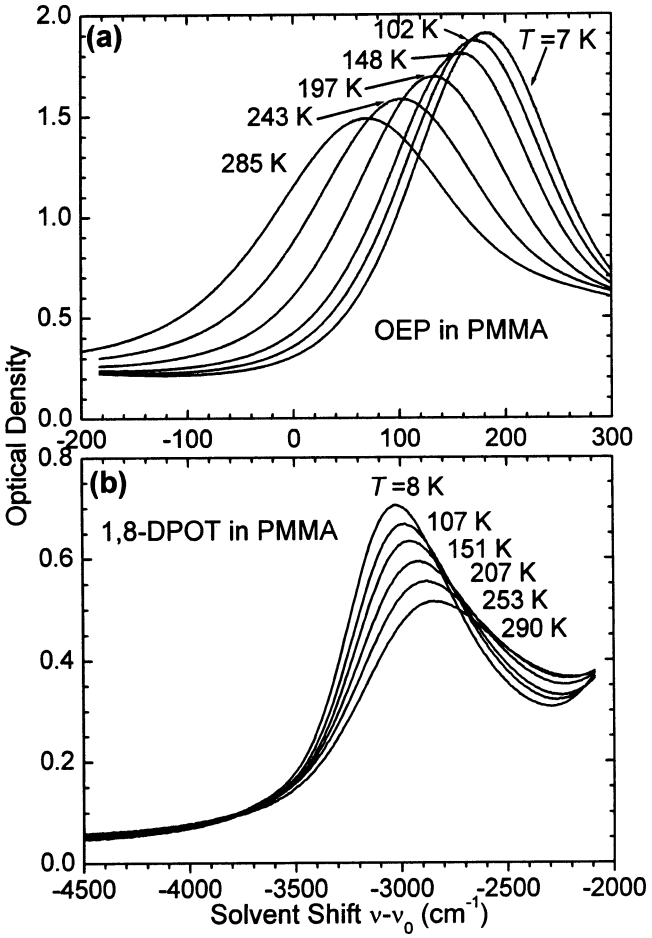

Figure 6. Temperature dependence of absorption spectra of octaethylporphine (a) and 1,8-diphenyloctatetraene (b) in poly(methyl methacrylate) films, plotted relative to 0−0 frequencies in a vacuum (16056 and 27732 cm^{-1}, respectively).

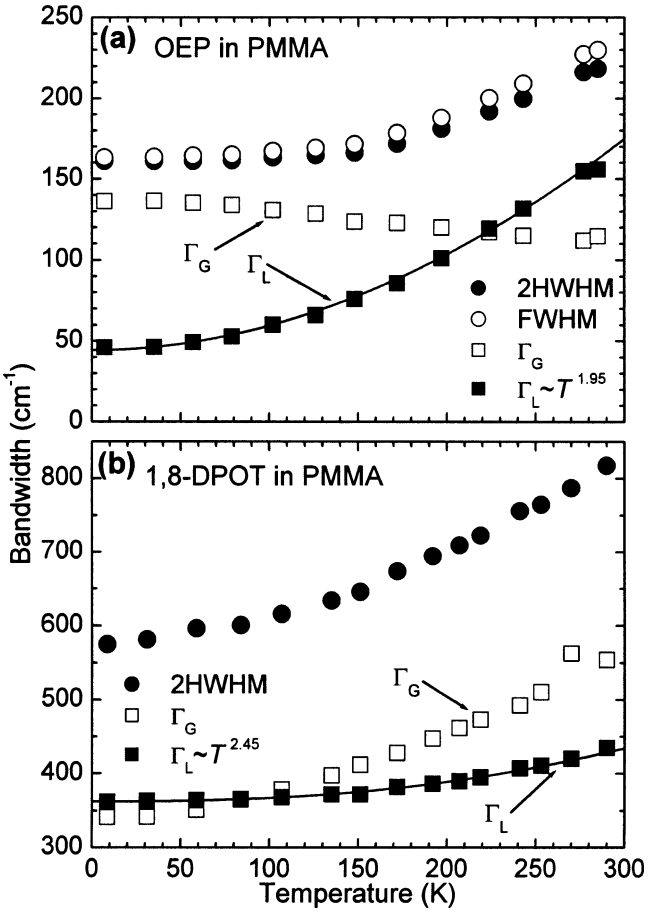

Figure 7. Temperature dependence of the absorption bandwidth and its Gaussian (Γ_G) and Lorentzian (Γ_L) components of OEP (a) and 1,8-DPOT (b) in PMMA.

frequencies in a vacuum ν_0 and the absolute solvent shifts $\Delta\nu_{max}$ ($\Delta\nu_{max} = \nu_{max} - \nu_0$) are summarized in Table 1 together with the thermal shift values between 6 and 100 (293) K. The band symmetry can be characterized by comparing the double half-width at half-maxima of the long-wavelength slope (2hwhm) with the full-width at half-maximum (fwhm). Most band shapes can very well be approximated to Voigt profiles over the whole *T* range. Voigtian treatment yields the widths of a Gaussian component, representing a steep, exponential decay, and a Lorentzian that has a shallow, hyperbolic falloff. The spectra were cut on the blue flank at 90% or 95% height of the peak maximum, and the low-frequency part, including the maximum, was subject to fitting. The bandwidth parameters 2hwhm, fwhm, Γ_G, and Γ_L are collected in Table 2 for the low-temperature spectra (6−10 K). The change of bandwidths between the lowest temperature and 100 (293) K are shown in parentheses. The *T* dependence of the above-mentioned four broadening parameters (2hwhm, fwhm, Γ_G, and Γ_L) is displayed in Figure 7 for OEP and 1,8-DPOT. The observed shifts of band maxima $\Delta\nu_{max}$ and its components (the pure thermal shift ν_T and the solvent shift ν_{solv}) of these chromophores are shown in Figure 8.

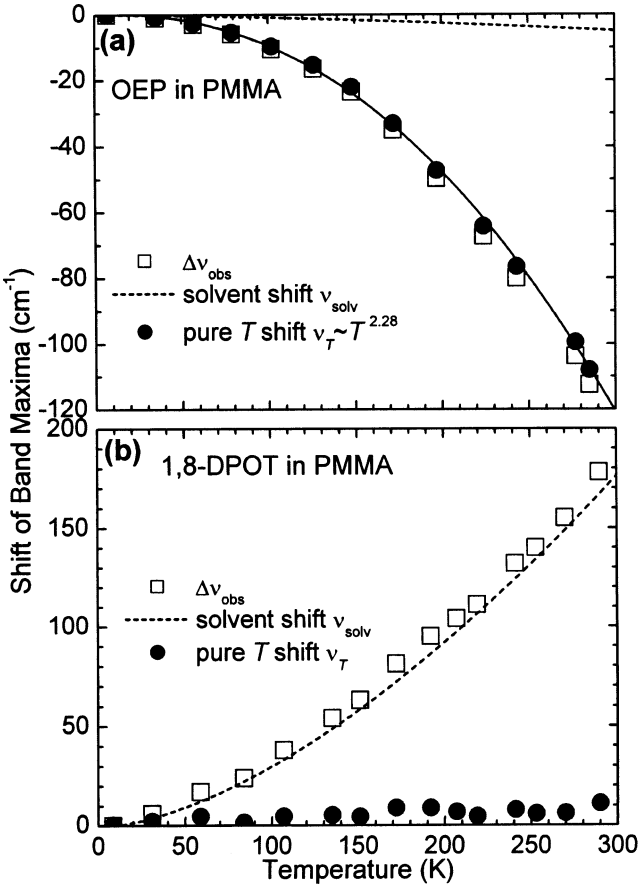

Figure 8. Temperature induced shift of absorption band maxima and its components in OEP (a) and 1,8-DPOT (b) in PMMA. Pure thermal shift ν_T is a difference between the observed shift and a solvent shift due to thermal expansion of matrix.

4. The Lennard-Jones Model

4.1. Structural Disorder and Inhomogeneous Broadening. Inhomogeneous bandwidth reflects the fluctuations of solvent shifts, resulting from the disorder in a guest−host system. Attractive dispersion (London) forces and exchange repulsion are the predominating interactions between nonpolar molecules, such as polyethylene and aromatic hydrocarbons. In terms of a Lennard-Jones (L-J) potential, the ground state stabilization energy (U_g) of an impurity molecule surrounded by solvent particles, each at a distance r_i, can be expressed as a sum of short-range repulsive and long-range attractive parts:

$$U_g = \epsilon_g \Sigma_i[(\sigma_g/r_i)^{12} - 2(\sigma_g/r_i)^6] \quad (2)$$

where ϵ_g is the depth of the potential well and σ_g is the distance between the solute and the solvent particles in the ground-state equilibrium. Three or nine sets of parameters ϵ_g and σ_g are needed, respectively, if either the solute or the solvent, or both are anisotropic.

In glasses, most intermolecular distances are close to equilibrium value, similar to that in the crystals. A small number of solvent particles deviating significantly from the equilibrium position are not only responsible for the vanishing of translational symmetry, but also have the largest contribution to local energy fluctuations. The sum sign may be dropped, if a single generalized coordinate is introduced:

$$U_g = \epsilon_g[(\sigma_g/r)^{12} - 2(\sigma_g/r)^6] \quad (3)$$

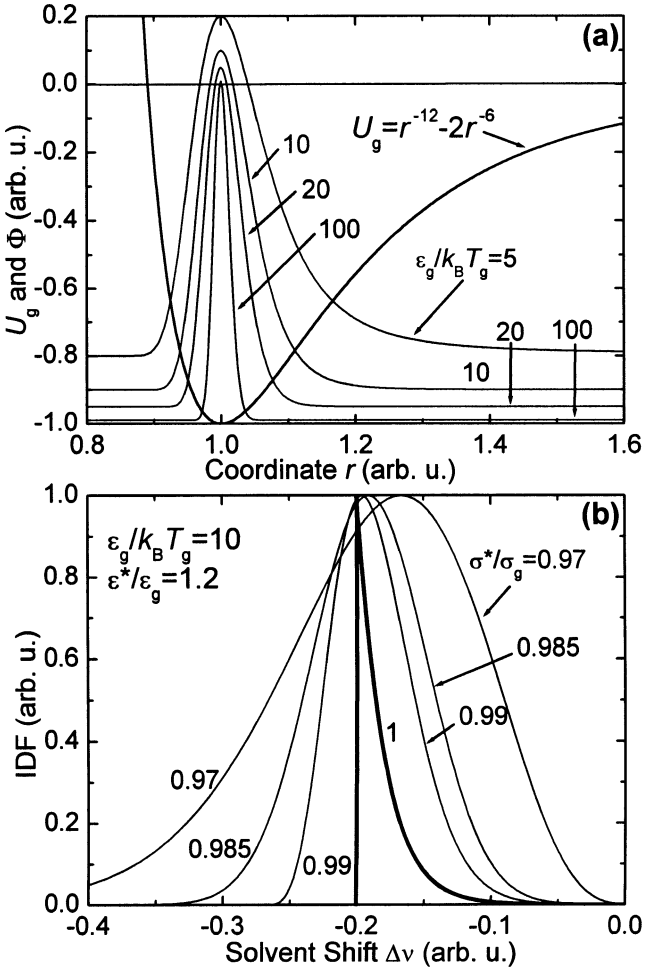

Figure 9. (a) Lennard-Jones potential and the Boltzmann energy distributions Φ for different glass transition temperatures (eq 4). The well-depths-to-thermal-energy ratio at glass temperature ϵ_g/k_BT_g equals to 5, 10, 20, and 100. Zero levels of distribution functions are shifted to match thermal energies k_BT_g above the potential minimum by 0.01, 0.05, 0.1, and 0.2 units, respectively. (b) Inhomogeneous bands (IDF) obtained from a ground-state energy distribution function with $\epsilon_g/k_BT_g = 10$ for different displacements of potential minima σ^*/σ_g. At $\sigma^*/\sigma_g = 1$ the largest possible negative solvent shift is −0.2, resulting in an unusual, one-sided distribution curve (thick line).

The L-J potential is often written in a slightly different form $U_g = 4\epsilon_g[(\sigma_g'/r)^{12} - (\sigma_g'/r)^6]$. Here σ_g' denotes a distance at which the potential energy changes sign. In the rigid sphere model σ_g' is often identified with a radius of the closest approach, or a diameter. Note that $\sigma_g = 2^{1/6}\sigma_g' = 1.12\sigma_g'$.

The solute−solvent interactions are degenerate in the sense that certain loose and tight guest−host configurations have the same energy. In disordered solids, the deviations from the equilibrium coordinate are frozen, due to very restricted structural relaxation below the glass temperature T_g. The particle distribution is established at the glass transition, so that the characteristic variation range of solvation energies is in the order of thermal energy k_BT_g. The Boltzmann distribution Φ of intermolecular interaction energies in the ground state can be written as

$$\Phi = \exp[-(U_g + \epsilon_g)/k_BT_g] \quad (4)$$

The distribution maximum is normalized at the well minimum by adding ϵ_g to the numerator of eq 4. Figure 9a shows a L-J potential for $\epsilon_g = \sigma_g = 1$ ($U_g = r^{-12} - 2r^{-6}$) and several distributions Φ for thermal energies by 5, 10, 20, and 100 times

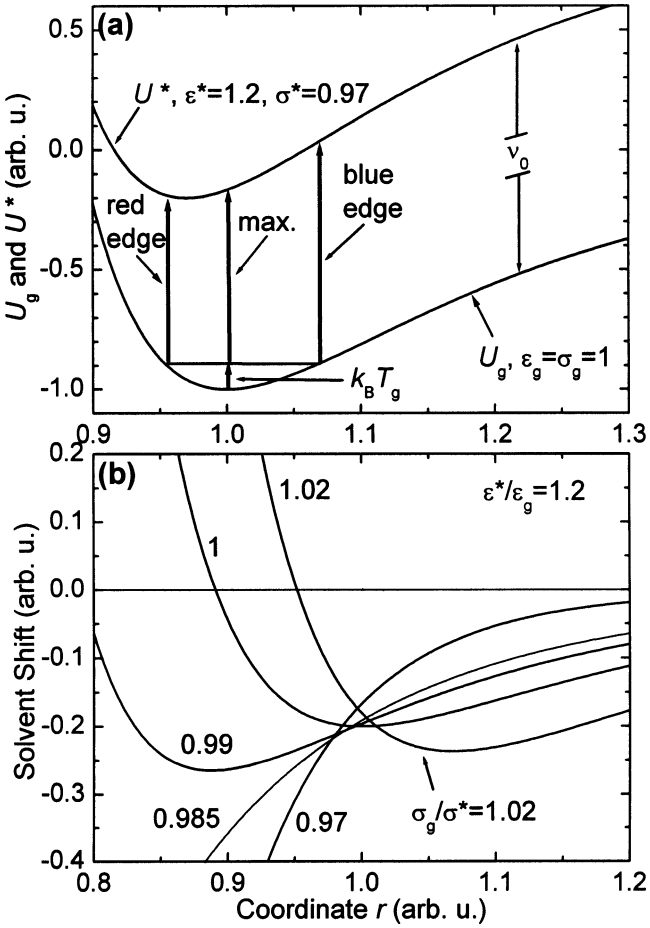

Figure 10. (a) Lennard-Jones potential surfaces of the ground state (U_g) and the excited state (U^*), ν_0 is the transition energy in a free guest molecule. Arrows denote optical transitions at the maximum and the edges of inhomogeneous band. (b) Vacuum-to-matrix shifts (solvent shifts) of transitions between a ground-state potential U_g ($\epsilon_g = \sigma_g = 1$) and the excited-state potentials U^* ($\epsilon^* = 1.2$) for different relative equilibrium positions σ^*/σ_g.

less than the well depth ϵ_g, respectively. When the fluctuation amplitude is small, the probability distribution Φ is a narrow Gaussian. In the materials with high glass temperatures, Φ becomes broad and asymmetrical.

To relate the distribution function Φ to the spread of optical transition energies (IDF), a potential function should be available for the excited state. The potential well is deeper in the excited state, because the $\pi-\pi^*$ and $n-\pi^*$ transitions in nonpolar chromophores are subject to negative (red, bathochromic) vacuum-to-matrix shifts. In addition, negative pressure shifts require the equilibrium coordinate be smaller in the upper state.[33] Therefore, out of four possibilities, the most relevant case with $\epsilon^* > \epsilon_g$ and $\sigma^* < \sigma_g$ is illustrated (Figure 10a). The potential curve of the excited state is upshifted by transition energy in a vacuum ν_0:

$$U^* = \epsilon^*[(\sigma^*/r)^{12} - 2(\sigma^*/r)^6] + \nu_0 \quad (5)$$

Absolute solvent shift $\Delta\nu$ (in energy units) is a difference between the potentials of the excited state (U^*) and the ground-state minus ν_0 (Figure 10b):

$$\Delta\nu = \nu - \nu_0 = U^* - U_g - \nu_0 \quad (6)$$

If the minima coincide, the largest solvent shift would occur at the equilibrium distance ($\sigma^* = \sigma_g$). The maximum (negative) solvent shift increases fast, if $\sigma^* \neq \sigma_g$, in particular, when $\sigma^* < \sigma_g$.

The inhomogeneous distribution of solvent shifts (IDF) is obtained by plotting the ground-state distribution Φ vs $\Delta\nu$, instead of r (Figure 9b). If the potential minima coincide ($\sigma^* = \sigma_g$), the degeneracy of the initial state is preserved also in transition energies, and the IDF would have a sharp cutoff of the red flank. The largest negative solvent shift would correspond to a potential minimum, whereas both the appressed and the loosely incorporated centers would absorb at higher frequencies. A small displacement of potential minima by 1% effectively removes the degeneracy in optical transition energies. The IDF is symmetrical and approximately Gaussian, if σ^*/σ_g equals to $(\epsilon_g/\epsilon^*)^{1/12}$, or 0.985 for $\epsilon^* = 1.2\epsilon_g$. The inhomogeneous band broadens fast with further decreasing the ratio σ^*/σ_g, and develops a shallow slope of the red flank. It is of interest that potential curves do not cross, when $(\epsilon_g/\epsilon^*)^{1/12} < \sigma^*/\sigma_g < (\epsilon_g/\epsilon^*)^{1/6}$; i.e., the relative coordinate shift lies between 0.97 and 0.985 in our example.

4.2. Pressure Dependence of Inhomogeneous Band Shape. Under hydrostatic and isotropic pressure all interparticle distances will be scaled to the same degree. Upon a linear compression by a factor of b, the potential energy amounts to

$$U_g' = \epsilon_g[(b\sigma_g/r)^{12} - 2(b\sigma_g/r)^6] \quad (7)$$

Here $b\sigma_g$ defines a new equilibrium position. It is easy to see that, besides the shifting to shorter distances, the width of ground-state energy distribution Φ is actually shrinking on compression:

$$\Phi = \exp[-(U_g' + \epsilon_g)/k_B T_g] \quad (8)$$

In contrast to the ground-state distribution function, the IDF broadens with increasing pressure, since the solvent shift has a steep distance dependence for $\sigma^*/\sigma_g < 0.99$ (Figure 10a). Apart from a broadening and a bathochromic shift, the changes in the band shapes are relatively small at high pressures (Figure 11). A pressure of 40 kbar causes a linear compression typically of 0.92 to 0.93 in many polymers and molecular crystals.[47,48] The broadening and the shift of the S_1 bands of phenanthrene and anthracene in PMMA matrix by a factor of 2−3 at 80 kbar[49] compare well with the predictions of the model, if the ratio of equilibrium distances σ^*/σ_g equals $(\epsilon_g/\epsilon^*)^{1/12}$ (0.985) rather than $(\epsilon_g/\epsilon^*)^{1/6}$ (0.97). Unfortunately, in the otherwise extensive literature on high-pressure spectroscopy the band shape analysis seems to be scarce, especially at low temperatures.[49−53]

4.3. Pressure Shift of Spectral Lines. The pressure shift of transition energy is obtained by differentiation of solvent shift (eq 6):

$$d\nu/dP = -12\epsilon^* r^{-1}(dr/dP)[(\sigma^*/r)^{12} - (\sigma^*/r)^6] + 12\epsilon_g r^{-1}(dr/dP)[(\sigma_g/r)^{12} - (\sigma_g/r)^6] \quad (9)$$

By introducing isothermal bulk compressibility β_T that is three times the linear compressibility α_T [$\alpha_T = -(dr/dP)_T r^{-1}$], one obtains

$$d\nu/dP = 4\beta_T[\epsilon^*(\sigma^*/r)^{12} - \epsilon^*(\sigma^*/r)^6 - \epsilon_g(\sigma_g/r)^{12} + \epsilon_g(\sigma_g/r)^6] \quad (10)$$

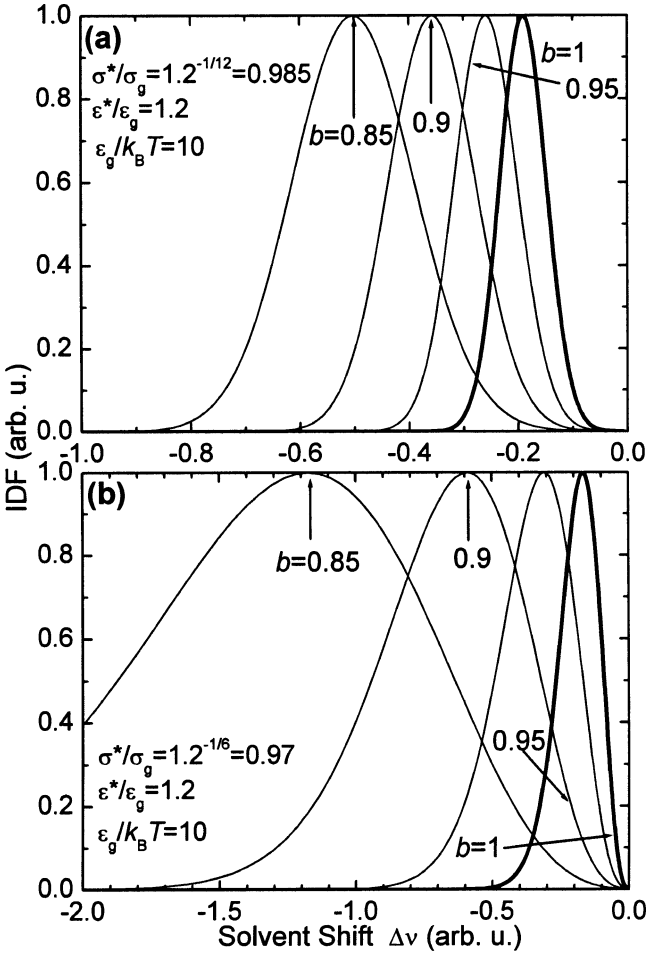

Figure 11. Pressure induced shift and broadening of inhomogeneous bands (IDF) for a ground-state energy distribution with $\epsilon_g/k_BT_g = 10$ and the displacements of potential minima σ^*/σ_g equal to 0.985 (a) and 0.97 (b) (see Figure 9b). The effect of linear compression b ranging from 1.0 to 0.85 is illustrated.

The slope a of a plot of pressure shift coefficients $d\nu/dP$ vs the solvent shift can be written as[33]

$$a = \frac{2\beta_T[2(\epsilon^*/\epsilon_g)(\sigma^*/r)^{12} - (\epsilon^*/\epsilon_g)(\sigma^*/r)^6 - 2(\sigma_g/r)^{12} + (\sigma_g/r)^6]}{[(\epsilon^*/\epsilon_g)(\sigma^*/r)^{12} - (\epsilon^*/\epsilon_g)(\sigma^*/r)^6 - (\sigma_g/r)^{12} + (\sigma_g/r)^6]} \quad (11)$$

If the ratio of potential well depths ϵ^*/ϵ_g scales either as $(\sigma_g/\sigma^*)^{12}$ or $(\sigma_g/\sigma^*)^6$ the slope values of $2\beta_T$ and $4\beta_T$ are obtained in the vicinity of the band maximum ($r = \sigma_g$). A numerical example with $\epsilon^*/\epsilon_g = 1.2$ shows that the pressure shift coefficients are nicely linear over a wide range of solvent shifts ($\Delta\nu$ is -0.2 at the band maximum) for shifted potential well minima with σ_g/σ^* equal to 0.97 or 0.985 (Figure 12a). The slopes between $2\beta_T$ and $4\beta_T$, as well as the deviation of $\nu_{0(P)}$ from the resonance frequency of a free chromophore ν_0 agree well with the P shift data in polymers[41] and ethanol glass.[42]

4.4. Temperature Shift and Broadening of Zero Phonon Lines. The line broadening and shift of dynamic origin at temperatures above 0 K are accounted for in terms of quadratic electron phonon coupling (QEPC). Both the dephasing rate and the line shift depend on a phonon frequency change, described with a quadratic term in harmonic potentials. The nonperturbative QEPC theory of Osadko[28] and Skinner[29] provides following expressions for the line shift ν_T and broadening Γ_h

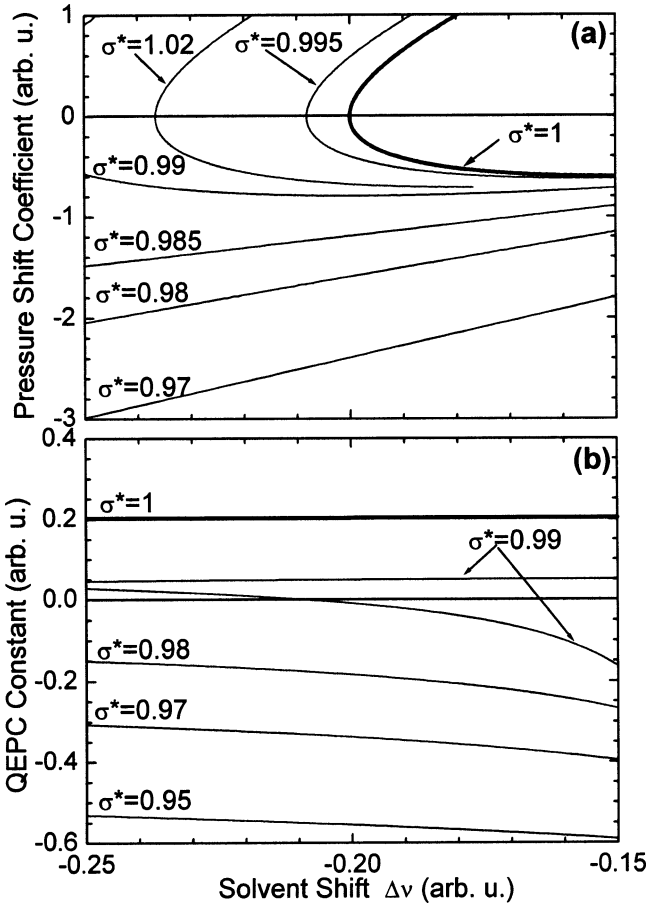

Figure 12. Dependence of pressure shift coefficients $d\nu/dP$ (a) and the quadratic electron−phonon coupling constants W (b) on solvent shift for different displacements of potential minima σ^*/σ_g. Very small relative displacements ($\sigma^*/\sigma_g \sim 1$) would lead to hole splitting.

(in frequency units) in the case of weak interaction with a single harmonic pseudolocal mode:

$$\nu_T = {}^1/_2 W\omega_g n(\omega_g) \quad (12)$$

$$\Gamma_h = {}^1/_4 W^2 \omega_g{}^2 \tau_g n(\omega_g)[n(\omega_g) + 1] \quad (13)$$

where W is the QEPC constant, ω_g is the phonon frequency, if the impurity is in the ground state, τ_g is the lifetime of the phonon level, and $n(\omega_g)$ is the Bose factor $\{n(\omega_g) = [\exp(h\omega_g/k_BT) - 1]^{-1}\}$.

In the low-temperature limit ($k_BT \ll h\omega_g$) one obtains from eqs 12 and 13 the same Arrhenius law [$\sim\exp(-h\omega_g/k_BT)$] for both the shift and the broadening. At high T ($k_BT \gg h\omega_g$), the Bose factors reduce to a linear and a quadratic dependence, respectively.

The QEPC constant W depends on the ratio of harmonic frequencies of a (pseudo)local vibration in the lower (ω_g) and the upper state (ω^*) as $(\omega^*/\omega_g)^2 - 1$. Therefore, W characterizes the curvature of potential energy surfaces. Localized phonons are known to interact particularly strongly with optical excitations. In crystals, the different mass and size of an impurity as well as changed force constants can cause phonon localization. On the other hand, in glasses, free volume plays additional and possibly predominating role in creating soft, localized modes.[34] A larger magnitude of effective coordinate r corresponds to a lower packing density of the host matrix, with decreased force constants between the particles. The second derivative of a potential $d^2U/dr^2 \equiv U''$ would yield a force constant k, that

determines the harmonic frequency as $\omega = (2\pi)^{-1}(k/\mu)^{1/2}$ (μ is the reduced mass). Thus, for L-J potentials, the QEPC constant can be expressed as[33]

$$W = U^{*\prime\prime}/U_g^{\prime\prime} - 1 = \{\epsilon^*[13(\sigma^*/r)^{12} - 7(\sigma^*/r)^6]/\epsilon_g[13(\sigma_g/r)^{12} - 7(\sigma_g/r)^6]\} - 1 \quad (14)$$

In Figure 12b W is plotted vs the solvent shift, rather than coordinate r. If the minima are not shifted, the QEPC constant at the band maximum ($r = \sigma_g = \sigma^*$) would depend only on the relative depth of potential wells as $\epsilon^*/\epsilon_g - 1$. For $\epsilon^*/\epsilon_g = 1.2$, the solvent shift at the band maximum is -0.2 and the thermal shift would be toward higher frequencies, since the QEPC constant W is positive (0.2). Therefore, a thermal blue shift is predicted for a transition with a red (negative) solvent shift, contrary to observations. When the potential wells are displaced, having σ^*/σ_g less than 0.98, bathochromic shifts may be obtained ($W < 0$). Moreover, a diminishing of negative temperature shifts with increasing (negative) solvent shift is evident, in agreement with the observed behavior of spectral holes (Figure 2).

5. Discussion

5.1. Pressure and Temperature Induced Shifts of Spectral Holes: A Frequency Dependence. Pressure shifts of spectral holes in glassy solvents and polymers have been extensively studied since 1987[54] (see Table 5 in ref 42 for a review of data). Transition frequencies of the chromophores in a vacuum and local compressibilities of several dye-doped proteins were derived, basing on an assumption that solely the dispersive interaction is responsible for the solvent shift.[55,56] However, the very fact of pressure induced broadening of holes indicates that this assumption is generally not valid, and therefore, additional interactions had to be considered.[41,42,57] For a single microscopic solvent shift mechanism the pressure shift is obviously proportional to the solvent shift. According to the London formula, the attractive dispersion energy depends on intermolecular distance as r^{-6} ($n = 6$), yielding a slope a equal to $2\beta_T$. However, a values as large as $4\beta_T$ ($12\alpha_T$) clearly indicate that a steeper intermolecular potential with a power coefficient around 12 is involved.[41,42] Large variation of a within a factor of 3 in PMMA[41] or ethanol glass,[42] doped with different dyes shows that a cannot be regarded as a matrix parameter. Moreover, the pressure shift vanishes at a frequency $\nu_{0(P)}$ that does not coincide with the 0−0 transitions measured in supersonic jets (Figure 2b). These inconsistencies have been resolved, at least in a qualitative level, by using a pair of displaced L-J type potentials (Figure 12a).[33] A correct (ascending) slope is obtained for the frequency dependence of P shift coefficients, if the steeper potential well of the upper state has a shorter equilibrium distance ($\sigma^* < \sigma_g$).

The L-J model using a single effective coordinate predicts no P shift at the band maximum, if the equilibrium positions coincide ($\sigma_g = \sigma^*$) (Figure 12a). By contrast, in the stochastic theory by Skinner, basing on the L-J potentials with $\sigma_g = \sigma^*$, a negative P shift originates from the displacement of solvent molecules in the outer coordination layers, with $r > \sigma_g$.[57] A gas like distribution of the host particles assumed in this model seems to be hard to reconcile with the fact that most particles occupying the first coordination sphere are located at $\sim\sigma_g$. The closest coordination layer should be considered in the first place, since it is responsible for at least of 90% of the solvent shift. The formal coordinate r used in our one-dimensional L-J model can be identified with an average distance of the closest neighbors surrounding the chromophore. In the context of phonon softening and localization, r can be associated also with a vacancy causing a deviation from σ_g. The equilibrium coordinates σ_g and σ^* depend on molecular wave functions of different electronic states, and cannot be regarded as independent variables.

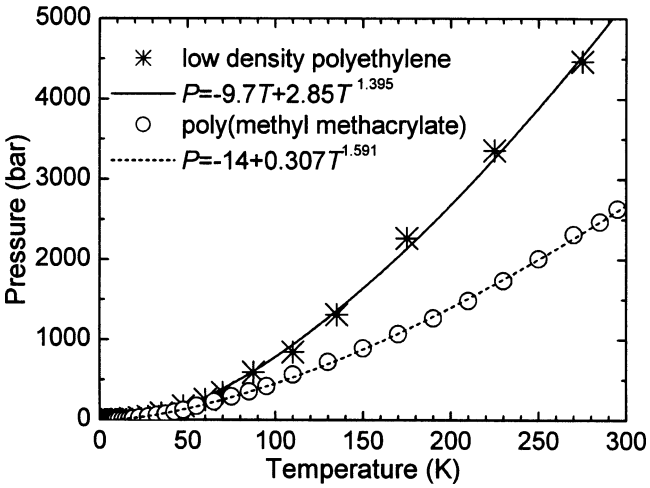

Figure 13. Isochores of the polymers, calculated from thermal expansion coefficients and isothermal compressibilities using eq 15.

A prominent dependence of temperature induced hole shifts on burning position has been reported recently (Figure 3).[43] The thermal shift is generally bathochromic, but becomes less negative on approaching the red edge of spectrum. The phonon-induced shift must be separated from the solvent shift component that is due to thermal expansion of the host matrix. The isochore was built by combining isobaric thermal expansion coefficient α_P with isothermal volume compressibility β_T (Figure 13):

$$P_V = \int_0^T (3\alpha_P/\beta_T)\, dT \quad (15)$$

Sufficiently accurate values of α_P in a broad T range are available for PMMA[58] and PE of different crystallinity.[59] Multiplication of $-P_V$ by a pressure shift coefficient $d\nu/dP$ yields a solvent shift ν_{solv} that is to be subtracted from the observed hole shift $\Delta\nu_{obs}$, to obtain the pure thermal, phonon-induced shift ν_T (Figure 3). The frequency dependence of ν_T between the burning T (6−8 K) and 25 or 35 K is plotted in Figure 2 (open squares). Pure thermal shift ν_T is predominately negative and has a weaker frequency dependence than $\Delta\nu_{obs}$ (Figure 3).

In quadratic EPC theory the thermal line shift is associated with the change of phonon frequencies in the respective electronic states (eq 12). A steeper potential well in the excited state, corresponding to a bathochromic solvent shift would obviously lead to a hypsochromic thermal shift. This controversy can be lifted, if the equilibrium coordinates are displaced in different electronic states. For $\sigma^* < \sigma_g$, a descending slope of the frequency dependence of ν_T is reproduced successfully (Figure 12b).

5.2. Pressure and Temperature Induced Broadening of Spectral Holes. As compared to hole shifts, the color effect in the broadening is weak. Pressure broadening coefficients $d\Gamma/dP$, the thermal hole broadening of holes burned at low T and the quasihomogeneous width Γ_{qh} all tend to be larger at the band edges, sometimes forming a shallow V-shape (Figure 2).[43] One-dimensional L-J model establishing a one-to-one relationship between the coordinate and the solvent shift can describe

only the shifts. Several degrees of freedom coupled with a two-branched potential are necessary for obtaining hole broadening as a result of isotropic compression or dilatation.[57] An important broadening mechanism could be the anisotropy of particles, requiring several sets of L-J parameters for adequate description of intermolecular interactions.

Negligible thermal shifts occurring on the red edge of OEP, TPP (Figure 3), or chlorin[43] spectra in both PMMA and PEld are in obvious contradiction with large broadening. Several QEPC constants with different signs, although producing a small net shift, could lead to a considerable broadening, since the homogeneous line width depends on W^2 (eq 13). Free volume, packing defects, and incongruous substitution can create a large number of quasilocal modes with different properties, covering a broad frequency interval. It would only be possible to distinguish in a single molecule experiment, whether a center couples to many modes simultaneously or interacts with a few (or just one) vibrations. However, a descending frequency dependence of thermal hole shifts proves that, on the average, the predictions of a single-mode model are fulfilled (Figure 12b).

5.3. Absorption Band Shape at the Low Temperature. In the low temperature limit, the observed band shape depends solely on the distribution of solvent shifts and the linear vibronic interactions, since the quadratic electron phonon coupling vanishes. Experimentally, IDF can be determined as a distribution of saturated depths of spectral holes or, preferably, by tuning the laser excitation within the 0−0 band, while recording the intensity of a well-defined vibronic line in fluorescence.[1−3] The IDF is difficult to measure accurately, if the zero-phonon lines are either weak or broad.

In the case of a symmetrical band the full-width at half-maximum (fwhm) and the double half-width at the low-frequency flank (2hwhm) coincide (Table 2). The fwhm has obviously little meaning, if intramolecular modes form strong vibronic satellites with intensities comparable to a 0−0 band, e.g., in pseudoisocyanine (PIC) or 9,10-dichloroanthracene (9,-10-ClA) (Figure 5). The low-frequency portion of the 0−0 band (2hwhm) has still been identified, very approximately, with IDF.[41,42] Remarkably, a nearly symmetrical Gaussian shape is obtained when the Franck−Condon factors are very large, such as in Phenol Blue. The progressions of high frequency 1200−1500 cm^{-1} core stretching vibrations combine with other local and pseudolocal modes, so that the spectral envelope loses all structure and merges into a band more than 2500 cm^{-1} wide (Figure 5). Such excessive broadening is diagnostic for charge-transfer transitions producing large shifts in the equilibrium coordinates of both intra- and intermolecular modes.

The long-wavelength portion of the spectrum, including the maximum, can almost perfectly be approximated to Voigt curves, enabling a partitioning to Gaussian (Γ_G) and Lorentzian (Γ_L) components. A large ratio Γ_G/Γ_L for Phenol Blue (∞), cryptocyanine (20.3), and chlorin (7.3) points to the prevalence of a Gaussian shape (Table 2). Extensive Lorentzian contribution in other systems indicates that most spectra fall off less steeply than the exponential law. Thermal broadening renders the spectra more Lorentzian, as indicated by a sharp decrease in the ratio Γ_G/Γ_L at room T (Table 2).

Inhomogeneous band shape calculated within the one-dimensional L-J model depends very strongly on the ratio of equilibrium coordinates σ^*/σ_g (Figure 9b). The low-frequency part of the calculated IDF curves was cut at 0.95 level on the blue side, similarly to the absorption spectra, and subject to a Voigt fitting. For $\sigma^*/\sigma_g = (\epsilon_g/\epsilon^*)^{1/6}$ equal to 0.97 in our example, the red flank has a considerable Lorentzian component of about 25%, with the ratio Γ_G/Γ_L equal to 3.8. An extending red flank and a more steeply rising blue side with 2hwhm/fwhm larger than unity occur in $\alpha(^1L_b)$-type transitions that are weakly coupled to low-frequency vibrations, e.g., in benzene, toluene, naphthalene, pyrene, and 3,4-benzopyrene (3,4-BP), even in liquid solutions. The role of electrostatic interactions is small in these transitions, and the host−guest potential is predominately of repulsive-dispersive type. Similar shapes have been reproduced by Kador[17] and Skinner[18] in a stochastic model using the L-J potentials with coincident minima, in apparent contradiction with our analysis.

With σ^*/σ_g approaching $(\epsilon_g/\epsilon^*)^{1/12}$, Γ_L decreases fast and the ratio Γ_G/Γ_L tends to infinity. The IDF is rendered a symmetrical Gaussian for $\sigma^*/\sigma_g = (\epsilon_g/\epsilon^*)^{1/12}$ (equal to 0.985 in Figure 9b). When the ratio σ^*/σ_g becomes even closer to unity, IDF develops a sharply rising low-frequency flank. In many spectra, the red flank is steeper than the high-frequency side (2hwhm/fwhm < 1), but this can mostly be a result of vibronic congestion, rather than IDF.

5.4. Temperature Narrowing of Inhomogeneous Width. The Voigtian analysis of absorption band shapes shows that the Gaussian width Γ_G can diminish with increasing temperature, in contrast to the bandwidth and its Lorentz component Γ_L (Table 2, Figure 7a). However, Γ_G increases for transitions with strong linear electron phonon coupling, as open-chain polymethine dyes (cryptocyanine and PICI) and 1,8-DPOT (Figure 7b). It follows from the L-J model (Figure 11) and the measurements at high pressure[49] that matrix compression enhances inhomogeneous bandwidth. As a consequence, the IDF that has been established at the glass transition is expected to broaden on cooling, and vice versa, a narrowing would occur on matrix expansion with increasing T.

Therefore, the narrowing of Γ_G can be associated with thermal volume expansion that can formally be related to a negative pressure $-P_V$, in accordance with the isochores of polymers. In eq 15 the volume compressibility β_T values at 4.2, 77, and 293 K, equal to 1.3, 1.35, and 1.48 are taken as linear with temperature for PMMA, whereas those of PEld, 1.41, 1.41 and 2.96, all in 10^{-5} bar^{-1} units,[60] respectively, were interpolated with an exponential growth. The isochores were approximated to power dependencies between 0 and 300 K (Figure 13). Pressure broadening coefficient of spectral holes $d\Gamma/dP$ multiplied by P_V yields a narrowing component $\Gamma_{ih}(P_{br})$. Another contribution to the shrinking of IDF, denoted as $\Gamma_{ih}(P_{sh})$ arises from the positive slope a of a frequency dependence of pressure shifts (Figure 2). Relative to the inhomogeneous bandwidth at low temperature Γ_{ih}, the narrowing can be written as a sum:

$$\Delta\Gamma_{ih} = -[\Gamma_{ih}(P_{br}) + \Gamma_{ih}(P_{sh})] = -(a\Gamma_{ih} + d\Gamma/dP)P_V \qquad (16)$$

Thermal volume expansion amounts to 3.7% in PMMA[58] and 9% in PEld at 293 K.[59] The volume shrinking on cooling to 0 K is equivalent to application of a pressure of 2.6 kbar on PMMA. The respective pressure is higher in PEld (4.9 kbar), because the thermal expansion at glass temperature (~240 K) is not fully compensated by the higher compressibility of the viscoelastic state. From a typical $d\Gamma/dP$ of 0.3 GHz/bar or 0.01 cm^{-1}/bar (Figure 2) and a "thermal pressure change" of −2.6 kbar one obtains the $\Gamma_{ih}(P_{br})$ of −26 cm^{-1} or roughly 10% of inhomogeneous bandwidth. The slope a varying between $2\beta_T$ and $4\beta_T$ (2.6×10^{-5} and 5.2×10^{-5} bar^{-1} in PMMA)[41] yields a relative change of inhomogeneous bandwidth $\Gamma_{ih}(P_{br})/\Gamma_{ih}$ of about 10%. In total, thermal expansion of the host matrix can

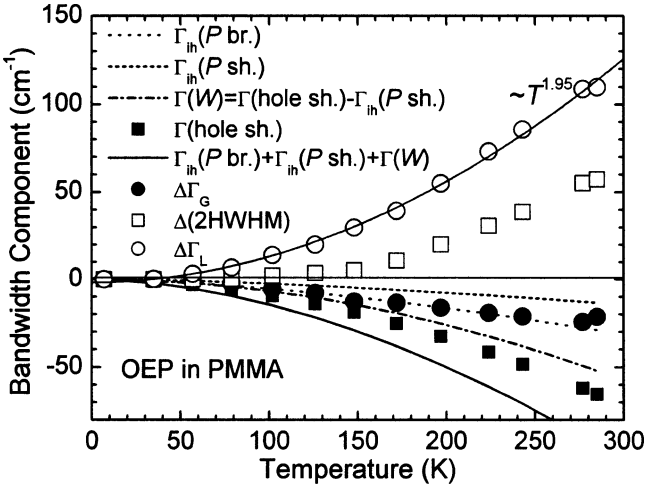

Figure 14. Temperature dependence of absorption bandwidth of OEP in PMMA, influenced by three narrowing components that are derived from the pressure broadening $\Gamma_{ih}(P_{br})$ (dotted line), the frequency dependence of pressure shifts $\Gamma_{ih}(P_{sh})$ (dashed line) and temperature shifts $\Gamma(W)$ (dash−dotted line) of zero-phonon holes. Total narrowing (thick line) is an overestimate as compared to the Gaussian narrowing $\Delta\Gamma_G$ (●), or the difference between the observed bandwidth 2hwhm (□) and the Lorentzian component $\Delta\Gamma_L$ (○) (not shown).

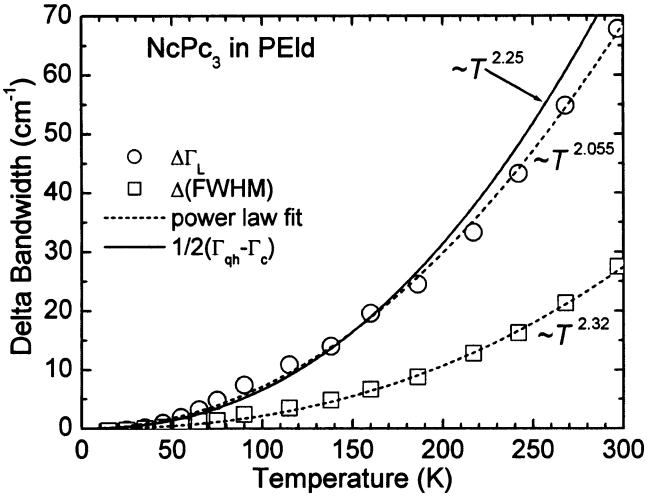

Figure 15. Temperature dependence of the band broadening Δ(fwhm) (□), its Lorentzian component $\Delta\Gamma_L$ (○) and the quasihomogeneous hole width Γ_{qh} for naphthalo-phthalocyanine in low-density polyethylene. Γ_{qh} was measured between 10 and 45 K, corrected for spectral diffusion broadening (eq 17, see Figure 4), and approximated to a power law (solid line).

result in band narrowing by ∼20% at 293 K, in qualitative accordance with the behavior of Γ_G in several dyes (Table 2, Figure 7a).

A question remains, however, whether the matrix dilatation influences solely the Gaussian part of the spectrum. A pressure change produces a Gaussian broadening of the initially Lorentzian spectral holes.[44,55] By contrast, a hole burned at high T retains a Lorentzian shape on cooling, despite of the broadening. Conservation of Lorentzian hole shapes was ascribed to a buildup of local, anisotropic strains at a T change.[44] The T dependence of mechanical properties reveals several relaxation processes in the polymers below T_g, referred to as α, β, γ, etc., transitions (α belongs to a glass transition).[61] Polyethylene is viscoelastic at room T, with T_g of about 240 K.[62,63] Notwithstanding the glass point above 293 K (T_g = 350 K), PMMA also remains pliable at ambient conditions. When soaked in liquid nitrogen (77 K) the polymers become very breakable (fragile) like mineral glass. Violent cracking on slight mechanical impact means that the surface energy of splinters should be compensated by relaxing internal strains. It is plausible that these strains accumulate only at temperatures considerably below T_g. Lorentzian hole broadening could be associated with anisotropy of such strains and their localization in the domains of nano- to micrometer size.[44] At the higher temperatures closer to T_g the thermal volume change is probably more isotropic, yielding a Gaussian broadening.

5.5. Electron—Phonon Coupling Effects on Bandwidth. Interestingly, another narrowing mechanism of the measured absorption contour follows from the frequency dependence of pure thermal, phonon-induced line shift ν_T that has the largest negative values on the high-frequency edge of spectrum (Figure 2). Bathochromic displacement of the blue flank of the spectrum with increasing T, combined with a negligible shift of the red edge, tends to squeeze the band (Figure 3). This additional mechanism is due to quadratic electron phonon coupling, and is independent from the microscopic solvent shifts, affecting inhomogeneous broadening. As a result, quadratic EPC contributes to the bandwidth in two opposite ways, via the dynamical broadening $\Gamma(W^2)$ and by means of frequency dependent shift ν_T that leads to a narrowing $\Gamma(W)$.

The interplay of different width components is illustrated in Figure 14 for S_1 absorption of octaethylporphine (OEP) in poly(methyl methacrylate). The observed hole shift $\Delta\nu_{obs}$ is a superposition of the solvent shift and the pure thermal shift ν_T (Figure 2). The bandwidth extrapolated from the frequency dependence of $\Delta\nu_{obs}$, denoted as Γ(hole shift) in Figure 14 (filled squares) is a sum of $\Gamma_{ih}(P_{sh})$ and the thermal shift effect $\Gamma(W)$, and thus, the latter can be derived as a difference. The narrowing component found from the pressure broadening of spectral holes $\Gamma_{ih}(P_{br})$ is occasionally quite similar to a change of the Gaussian width $\Delta\Gamma_G$ (filled circles). The observed broadening Δ(2hwhm) (open squares) is remarkably small below 150 K as compared to the Lorentzian broadening $\Delta\Gamma_L$ (open circles), thus giving a direct evidence for the narrowing processes.

Bearing in mind the presumably dynamical nature of Lorentzian broadening $\Delta\Gamma_L$, a comparison with the extrapolated (quasi)homogeneous hole width Γ_{qh} would be of interest. The width of a resonant fluorescence line, or a hole, excited with monochromatic light, would correspond to a double homogeneous width, as a result of self-convolution of two identical Lorentzians. Hole broadening caused by spectral diffusion Γ_c is to be subtracted from Γ_{qh}, to obtain a theoretically relevant dynamic width (eq 13):

$$\Gamma_h = {}^1/_2(\Gamma_{qh} - \Gamma_c) \qquad (17)$$

Temperature dependencies of Δ(fwhm), $\Delta\Gamma_L$, and the extrapolated homogeneous line width Γ_h are compared in Figure 15 for phthalonaphthalocyanine ($NcPc_3$) in a low-density polyethylene matrix. The Γ_{qh} measured between 10 and 45 K was corrected for the spectral diffusion (eq 17, see Figure 4) and approximated to a power law as $T^{2.25}$ (solid line). The Lorentzian broadening $\Delta\Gamma_L$ and the extrapolated Γ_h compare surprisingly well up to 300 K. Tentatively, one can assume that $\Delta\Gamma_L$ indeed reflects the rate of dephasing over a broad temperature range.

In many chromophores $\Delta\Gamma_L$ varies between 70 and 290 cm^{-1} at 293 K. The temperature coefficients of a power-law fit a_2-(Γ_L) are rather uniform, 2.1 ± 0.3 (Table 2). On the other hand, the as-measured broadening Δ(2hwhm) ranges between 30 and 300 cm^{-1} at 293 K, and the fit coefficients show a much larger scatter of 2.4 ± 0.7 (Table 2).

The influence of linear electron−phonon coupling on broadening is undoubtedly strong, but difficult to assess. The phonon assisted anti-Stokes absorption on the low-frequency side of 0−0 line contributes to overall broadening at $T > 0$. The Debye−Waller factors are obviously small ($\alpha < 0.01$) in the flexible chromophores with high densities of internal low-frequency modes (PICI, 1,8-DPOT) or a charge-transfer transition (Phenol Blue). The respective Huang−Rhys factor (equal to $-\ln\alpha$) shows that at least five phonons will be created on electronic excitation. It appears that linear EPC contributes predominately to the Gaussian component, and masks the decrease of Γ_G in the chromophores with strong vibronic coupling (Figure 7b).

Consequently, a partitioning scheme can be proposed for the *T*-dependent bandwidth, on the basis of linear EPC [$\Delta\Gamma$(LEPC)], quadratic EPC [$\Gamma(W^2)$ and $\Gamma(W)$], and a change of inhomogeneous distribution function [$\Gamma_{ih}(P_{br}) + \Gamma_{ih}(P_{sh})$]:

$$\Delta\Gamma(2\text{hwhm}) = \Delta\Gamma(\text{LEPC}) + \Gamma(W^2) - [\Gamma(W) + \Gamma_{ih}(P_{br}) + \Gamma_{ih}(P_{sh})] \quad (18)$$

The homogeneous broadening is mainly Lorentzian, while the linear EPC and the shrinking of IDF predominately affect the Gaussian part. The determination of dephasing rates in terms of $\Delta\Gamma_L$ is of considerable interest, because the homogeneous line width is hardly accessible by burning persistent spectral holes at high temperatures (50−300 K).

5.6. Temperature Shift of the Absorption Band Maxima. It has been reckognized for a some time that the spectral shifts induced by a temperature change should have a component that depends on matrix density.[54,64] The solvent shift caused by thermal expansion was estimated on the basis of pressure shift coefficients and the "thermal pressure" derived from the isochore equation (eq 15). Pure thermal shift ν_T is calculated from the observed shift $\Delta\nu_{obs}$ and the solvent shift:

$$\nu_T = \Delta\nu_{obs} + (d\nu_{max}/dP)P_V \quad (19)$$

Pressure shift coefficients of spectral holes burned at the band maximum $d\nu_{max}/dP$ are available for a number of chromophores.[41] For other compounds $d\nu_{max}/dP$ can be estimated from the correlations with solvent shifts $\Delta\nu_{max}$ (see Figure 9 in ref 41) or, preferably, slopes of solvatochromic plots *p* (Table 1):

$$d\nu_{max}/dP = (0.020 \pm 0.06) + (1.99 \pm 0.30) \times 10^{-4} p; \quad R = 0.937, \quad n = 8 \quad (20)$$

The slope *p* expresses the sensitivity of spectral transition energies with respect to the Lorentz−Lorenz function of refractive index (solvent polarizability) in liquids at ambient temperature.[39,42,46]

For the majority of transitions the phonon induced shifts ν_T are negative and vary within a relatively narrow range, between -8 and -14 cm^{-1} at 100 K and -64 and -146 cm^{-1} at 293 K (Table 1). In contrast, the solvent shift component ν_{solv} is hypsochromic and reflects simply a reversal of bathochromic solvent and pressure shifts with the dilatation of matrix. For many transitions with moderately large dispersive solvent shifts varying between -600 and -1300 cm^{-1} (phthalocyanine, p-bands of polyarenes, cyanine dyes) ν_{solv} and ν_T are approximately equal, but with opposite signs, so that a mutual cancellation takes place (Table 1). As a result, the observed band shifts are small and irregular. By contrast, in 1,8-DPOT and Phenol Blue characterized with huge solvent shifts exceeding -3000 cm^{-1}, ν_T can be small (Figure 8b) or even positive. One may speculate, that in 1,8-DPOT, with high polarizability in the excited state (reflected in the *p* value as large as -10^4 cm^{-1}) that corresponds to an extended electron distribution, the intermolecular equilibrium coordinate σ^* is not less than σ_g, and as a consequence, $W > 0$ (eq 14, Figure 12b).

The power coefficients of *T* shifts of are quite uniform (2.0 ± 0.3) and close to those for the Lorentzian broadening (2.1 ± 0.3) (Tables 1 and 2). Therefore, a single mode approach in a weak coupling limit (eqs 12 and 13), predicting a linear and a quadratic dependence for the shift and broadening at the high *T* limit, respectively, is not sufficient for the description of molecular materials in a broad *T* interval. Internal degrees of freedom in large molecules, covering a wide range of frequencies can evidently play an important role in quadratic EPC processes.

Negative thermal shifts may seem incompatible with vacuum-to-matrix shifts of the same sign, because a bathochromic solvent shift presupposes a stabilization of the excited state. A steeper potential well of the upper state has a higher frequency, resulting in a positive coupling constant *W* (eq 14). This paradox can be resolved within the L-J model, if the equilibrium distances are shorter in the excited states ($\sigma^* < \sigma_g$, Figure 12b).

5. Conclusions

A comparative study of broadband absorption spectra and spectral holes was carried out for organic chromophores embedded in glassy polymers. Quite obviously, thermal shifts of the spectra constitute a superposition of a phonon induced shift, and a solvent shift depending on a density change of the host matrix. It was established for the first time that the matrix expansion also causes shrinking of inhomogeneous bandwidth, thus explaining unusually small band broadening in several guest−host systems. A decrease of the Gaussian component of the spectrum with increasing temperature can be directly ascertained for transitions with appreciable zero phonon lines. The narrowing mechanisms manifest themselves in the baric shift and broadening of zero phonon holes burned within inhomogeneous band. Additional narrowing arises as a result of the frequency dependence of pure thermal, phonon induced line shifts.

The absorption contour is rarely a pure Gaussian, and contains a substantial Lorentz component, even at 5 K. Thermal broadening of the latter is comparable with the hole broadening, corrected for spectral diffusion and extrapolated far beyond the actual burning temperature range of 6 to 50 K up to 300 K. Thus, Lorentzian broadening is largely homogeneous, and due to quadratic interaction with phonons. Linear vibronic coupling in the form of anti-Stokes transitions gives rise to predominately Gaussian broadening.

Characteristic dependencies of thermal and baric hole shifts on burning position, having opposite slopes, could be successfully reproduced in terms of Lennard-Jones potentials containing a single effective coordinate. Non-Gaussian inhomogeneous band shapes and their transformation on matrix compression can also be accounted for. In the excited-state equilibrium the intermolecular distances must be less for bathochromically shifted transitions.

Acknowledgment. This work was supported by the Estonian Science Foundation, Grant No. 6546.

References and Notes

(1) Kikas, J. *Chem. Phys. Lett.* **1978**, *57*, 511.
(2) Kikas, J. V.; Treshchalov, A. B. *Chem. Phys. Lett.* **1983**, *98*, 295.

(3) Renge, I.; Wild, U. P. *J. Lumin.* **1996**, *66&67*, 305.
(4) Basché, T., Moerner, W. E., Orrit, M., Wild, U. P., Eds. *Single-Molecule Optical Detection, Imaging* and Spectroscopy; VCH: Weinheim, Germany, 1997.
(5) Myers, A. B.; Tchénio, P.; Zgierski, M. Z.; Moerner, W. E. *J. Phys. Chem.* **1994**, *98*, 10377.
(6) Kozankiewicz, B.; Bernard, J.; Orrit, M. *J. Chem. Phys.* **1994**, *101*, 9377.
(7) Caruge, J.-M.; Orrit, M. *Phys. Rev. B* **2001**, *64*, 205202.
(8) Hofmann, C.; Ketelaars, M.; Matsushita, M.; H. Michel, H.; Aartsma, T. J.; Köhler, J. *Phys. Rev. Lett.* **2003**, *90*, 013004.
(9) Moerner, W. E., Ed. *Persistent Spectral Hole-Burning: Science and Applications*; Springer: Berlin, 1988.
(10) Sild, O.; Haller, K., Eds. *Zero-Phonon Lines and Spectral Hole Burning in Spectroscopy and* Photochemistry; Springer: Berlin, 1988.
(11) Basu, S. *Adv. Quantum Chem.* **1964**, *1*, 145.
(12) Bakshiev, N. G.; Girin, O. P.; Piterskaya, I. V. *Opt. Spektrosk.* **1968**, *24*, 901 [*Opt. Spectrosc.* **1968**, *24*, 483].
(13) Mataga, N.; Kubota, T. *Molecular Interactions and Electronic Spectra*; Marcel Dekker: New York, 1970.
(14) Cossi, M.; Barone, V. *J. Chem. Phys.* **2001**, *115*, 4708.
(15) Stoneham, A. M. *Rev. Mod. Phys.* **1969**, *41*, 82.
(16) Leontidis, E.; Suter, U. W.; Schütz, M.; Lüthi, H.-P.; Renn, A.; Wild, U. P. *J. Am. Chem. Soc.* **1995**, *117*, 7493.
(17) Kador, L. *J. Chem. Phys.* **1991**, *95*, 5574.
(18) Sevian, H. M.; Skinner, J. L. *Theor. Chim. Acta* **1992**, *82*, 29.
(19) Rebane, K. K. *Impurity Spectra of Solids*; Plenum: New York, 1970.
(20) Maradudin, A. A. *Solid State Phys.* **1966**, *18*, 273.
(21) Osad'ko, I. S. In *Spectroscopy and Excitation Dynamics of Condensed Molecular Systems*; Agranovich, V. M., Hochstrasser, R. M., Eds.; North-Holland: Amsterdam, 1982.
(22) Rebane, K. K.; Khizhnyakov, V. V. *Opt. Spektrosk.* **1963**, *14*, 362 [*Opt. Spectrosc.* **1963**, *14*, 193].
(23) McCumber, D. E.; Sturge, M. D. *J. Appl. Phys.* **1963**, *34*, 1682.
(24) Imbush, G. F.; Yen, W. M.; Schawlow, A. L.; McCumber, D. E.; Sturge, M. D. *Phys. Rev.* **1964**, *133*, A1029.
(25) de Bree, P.; Wiersma, D. A. *J. Chem. Phys.* **1979**, *70*, 790.
(26) Silbey, R.; Kassner, K. *J. Lumin.* **1987**, *36*, 283.
(27) Hizhnyakov, V. *J. Phys. C: Solid State Phys.* **1987**, *20*, 6073.
(28) Osad'ko, I. S. *Phys. Reports* **1991**, *206*, 43.
(29) Skinner, J. L.; Hsu, D. *Adv. Chem. Phys.* **1986**, *65*, 1.
(30) Ariese, F., Gooijer, C., Hofstraat, H.; Eds. *Shpol'skii Spectroscopy and Other Site Selection Methods: Application in Environmental Analysis, Bioanalytical Chemistry, and Chemical Physics*; Wiley Series on Chemical Analysis 156; Wiley: New York, 2000.
(31) Reichardt, C. *Solvents and Solvent Effects in Organic Chemistry*; Wiley-VCH: Weinheim, Germany, 2003.
(32) Koppel, I. A.; Palm, V. A. In *Advances in Linear Free Energy Relationships*; Chapman, N. B., Shorter, J., Eds.; Plenum: London, 1972; pp 203−280.
(33) Renge, I. *J. Phys. Chem. B* **2004**, *108*, 10596.
(34) Renge, I. *Chem. Phys. Lett.* **2005**, *405*, 404.
(35) Even, U.; Magen, J.; Jortner, J.; Friedman, J.; Levanon, H. J. *J. Chem. Phys.* **1982**, *77*, 4374.
(36) Even, U.; Jortner, J. *J. Chem. Phys.* **1982**, *77*, 4391.
(37) Löhmannsröben, H.-G.; Bahatt, D.; Even, U. *J. Phys. Chem.* **1990**, *94*, 4025.
(38) Menapace, J. A.; Bernstein, E. R. *J. Chem. Phys.* **1987**, *87*, 6877.
(39) Renge, I.; Wolleb, H.; Spahni, H.; Wild, U. P. *J. Phys. Chem. A* **1997**, *101*, 6202.
(40) Renge, I. *J. Chem. Phys.* **1997**, ***106***, 5835.
(41) Renge, I. *J. Phys. Chem. A* **2000**, *104*, 3869.
(42) Renge, I. *J. Phys. Chem. A* **2000**, *104*, 7452.
(43) Renge, I. *Phys. Rev. B* **2003**, *68*, 064205.
(44) Renge, I. *Chem. Phys. Lett.* **2002**, *357*, 409.
(45) Schulte, G.; Grond, W.; Haarer, D.; Silbey, R. *J. Chem. Phys.* **1988**, *88*, 679.
(46) Renge, I. *J. Photochem. Photobiol. A: Chem.* **1992**, *69*, 135.
(47) Bridgman, P. W. *Proc. Am. Acad. Arts Sci.* **1948**, *76*, 71.
(48) Vaidya, S. N.; Kennedy, G. C. *J. Chem. Phys.* **1971**, *55*, 987.
(49) Okamoto, B. Y.; Drickamer, H. G. *J. Chem. Phys.* **1974**, *61*, 2870.
(50) Drickamer, H. G. *Annu. Rev. Phys. Chem.* **1982**, *33*, 25.
(51) Offen, H. W. In *Organic Molecular Photophysics*, Birks, J. B., Ed.; Wiley: London, 1973; pp 103−151.
(52) Zhu, A.; Mio, M. J.; Moore, J. S.; Drickamer, H. G. *J. Phys. Chem. B* **2001**, *105*, 3300.
(53) Drotning, W. D.; Drickamer, H. G. *Phys. Rev. B* **1976**, *13*, 4568.
(54) Sesselmann, Th.; Richter, W.; Haarer, D.; Morawitz, H. *Phys. Rev. B* **1987**, *36*, 7601.
(55) Gradl, G.; Zollfrank, J.; Breinl, W.; Friedrich, J. *J. Chem. Phys.* **1991**, *94*, 7619.
(56) Lesch, H.; Schlichter, J.; Friedrich, J.; Vanderkooi, J. M. *Biophys. J.* **2004**, *86*, 467.
(57) Laird, B. B.; Skinner, J. L. *J. Chem. Phys.* **1989**, *90*, 3274.
(58) Lyon, K. G.; Salinger, G. L.; Swenson, C. A. *Phys. Rev. B* **1979**, *19*, 4231.
(59) White, G. K.; Choi, C. L. *J. Polym. Sci.: Polym. Phys. Ed.* **1984**, *22*, 835.
(60) Perepechko, I. I. *Low-Temperature Properties of Polymers*; Mir Publishers: Moscow, 1980; p 272.
(61) Sauer, J. A.; Saba, R. G. J. *Macromol. Sci.—Chem.* **1969**, *A3*, 1217.
(62) van Krevelen, D. W. *Properties of Polymers*; Elsevier: Amsterdam, 1990.
(63) Brandrup, J.; Immergut, H., Eds.; *Polymer Handbook*, 3rd ed.; Wiley: New York, 1989.
(64) Laisaar, A. I.; Mugra, A. K.-I.; Sapozhnikov, M. N. *Fiz. Tverd. Tela* **1974**, *16*, 1155 [*Sov. Phys. Solid State* **1974**, *16*, 741].